Correspondence

Bayesian NDE Defect Signal Analysis

Aleksandar Dogandžić and Benhong Zhang

***Abstract*—We develop a hierarchical Bayesian approach for estimating defect signals from noisy measurements and apply it to nondestructive evaluation (NDE) of materials. We propose a parametric model for the shape of the defect region and assume that the defect signals within this region are random with unknown mean and variance. Markov chain Monte Carlo (MCMC) algorithms are derived for simulating from the posterior distributions of the model parameters and defect signals. These algorithms are then utilized to identify potential defect regions and estimate their size and reflectivity parameters. Our approach provides Bayesian confidence regions (credible sets) for the estimated parameters, which are important in NDE applications. We specialize the proposed framework to elliptical defect shape and Gaussian signal and noise models and apply it to experimental ultrasonic C-scan data from an inspection of a cylindrical titanium billet. We also outline a simple classification scheme for separating defects from nondefects using estimated mean signals and areas of the potential defects.**

***Index Terms*—Bayesian analysis, defect estimation and detection, Markov chain Monte Carlo (MCMC) methods, nondestructive evaluation (NDE).**

I. Introduction

In nondestructive evaluation (NDE) applications, defect signal typically affects multiple measurements at neighboring spatial locations. Therefore, multiple spatial measurements should be incorporated into defect detection and estimation (sizing) algorithms. In [1], measurements within a sliding window were compared with a dynamically chosen threshold in order to detect potential defects in ultrasonic C scans. Related problems have been studied in image processing literature in the context of image segmentation and saliency region detection, see e.g., [2]–[4] (respectively) and references therein. In this correspondence (see also [5]), we propose the following:

- a *parametric model* that describes defect shape, location, and reflectivity;
- a *hierarchical Bayesian* framework and Markov chain Monte Carlo (MCMC) algorithms for estimating these parameters assuming a singe defect;
- a sequential method for identifying multiple potential defect regions and estimating their parameters;
- a simple classification scheme for separating defects from nondefects using estimated mean signals and areas of the potential defects.

We adopt elliptical defect shape and Gaussian signal and noise models; however, the proposed framework is applicable to other scenarios as well. The elliptical shape model is well-suited for describing hard alpha inclusions in titanium alloys [6]. In most applications, the defect signal is not uniform over the defect region but varies *randomly* depending, for example, on local reflectivity and various constructive and destructive interferences. To account for these variations, we assume that the defect signal is *random* over the defect region, having fixed (but unknown) mean and variance.

In Section II, we describe the measurement model and prior specifications. In Section III and Section A of the Appendix, we develop Bayesian methods for simulating and estimating the defect model parameters and signals (Sections III-A–III-C). In addition, our approach provides *Bayesian confidence regions (credible sets)* for the estimated parameters, which are important in NDE applications. The underlying Bayesian paradigm allows us to easily incorporate available prior information about the defect reflectivity, shape, or size. In Section IV, the proposed methods are applied to experimental ultrasonic C-scan data from an inspection of a cylindrical titanium billet. Although we focus on estimating parameters of a single defect, we also discuss the multiple-defect scenario in Section IV. Note that applying optimal Bayesian approaches for estimating the number and parameters of multiple defects (e.g., reversible-jump MCMC schemes [9, Ch. 11]) would lead to computationally intractable solutions. In Section IV, we propose a simple sequential method and a classification scheme for identifying multiple potential defect regions and separating defects from nondefects. Concluding remarks are given in Section V.

II. Measurement Model and Prior Specifications

We first introduce our parametric defect location and shape models (Section II-A) and random noise and defect-signal models (Sections II-B and II-C). Then, in Section II-D, we combine the noise and signal models by integrating out the random signals. Our goal is to estimate the model (defect location, shape, and signal-distribution) parameters and random signals. In Section II-E, we introduce our model-parameter prior specifications.

The random defect signals and model parameters that we wish to estimate are described using a *hierarchical statistical model*, see [7, Ch. 5] for an introduction to hierarchical models.

A. Parametric Model for Defect Location and Shape

Assume that a potential defect-signal region $\mathcal{R}(\boldsymbol{z})$ can be modeled as an ellipse, as follows:

$$\mathcal{R}(\boldsymbol{z}) = \left\{ \boldsymbol{r} : (\boldsymbol{r}-\boldsymbol{r}_0)^T \Sigma_{\mathrm{R}}(d,A,\varphi)^{-1} (\boldsymbol{r}-\boldsymbol{r}_0) \le 1 \right\} \tag{2.1}$$

where $\boldsymbol{r} = [x_1, x_2]^T$ denotes location in Cartesian coordinates,

$$\boldsymbol{z} = \left[\boldsymbol{r}_0^T, d, A, \varphi \right]^T \tag{2.2}$$

is the vector of (unknown) defect location and shape parameters,[1]

$$\Sigma_{\mathrm{R}}(d,A,\varphi) = \Phi(\varphi) \cdot \begin{bmatrix} d^2 & 0 \\ 0 & A^2/(d^2\pi^2) \end{bmatrix} \cdot \Phi(\varphi)^T,$$
$$\Phi(\varphi) = \begin{bmatrix} \cos\varphi & -\sin\varphi \\ \sin\varphi & \cos\varphi \end{bmatrix} \tag{2.3}$$

[1]The inverse of Σ_{R} can be easily computed as $\Sigma_{\mathrm{R}}(d,A,\varphi)^{-1} = \Phi(\varphi) \cdot \begin{bmatrix} 1/d^2 & 0 \\ 0 & d^2\pi^2/A^2 \end{bmatrix} \cdot \Phi(\varphi)^T$.

Manuscript received September 5, 2005; revised February 6, 2006. The associate editor coordinating the review of this manuscript and approving it for publication was Prof. Steven M. Kay. This work was supported by the NSF Industry-University Cooperative Research Program, Center for Nondestructive Evaluation, Iowa State University.

The authors are with the Department of Electrical and Computer Engineering, Iowa State University, Ames, IA 50011 USA (e-mail: ald@iastate.edu; zhangbh@iastate.edu).

Digital Object Identifier 10.1109/TSP.2006.882064

and "^{T}" denotes a transpose. Here, $\boldsymbol{r}_0 = [x_{0,1}, x_{0,2}]^T$ represents the center of the ellipse in Cartesian coordinates, $d > 0$ is an axis parameter, $A > 0$ the area of the ellipse, and $\varphi \in [-\pi/4, \pi/4]$ the ellipse orientation parameter (in radians). Under the above parametrization, d and $A/(d\pi)$ are the axes of the ellipse $\mathcal{R}(\boldsymbol{z})$.

B. Measurement-Error (Noise) Model

Assume that we have collected measurements y_i at locations $\boldsymbol{s}_i$, $i = 1, 2, \ldots, \mathbb{N}_{\text{tot}}$ within the region of interest, where $\mathbb{N}_{\text{tot}}$ denotes the total number of measurements in this region. We adopt the following measurement-error model.

- If y_i is collected over the defect region (i.e. $\boldsymbol{s}_i \in \mathcal{R}(\boldsymbol{z})$), then

$$y_i = \theta_i + e_i \tag{2.4a}$$

  where θ_i and e_i denote the defect signal (related to its reflectivity) and noise at location $\boldsymbol{s}_i$, respectively.
- If y_i is collected outside the defect region (i.e., $\boldsymbol{s}_i \in \mathcal{R}^{\text{c}}(\boldsymbol{z})$, where $\mathcal{R}^{\text{c}}(\boldsymbol{z})$ denotes the *noise-only region* outside $\mathcal{R}(\boldsymbol{z})$), then the measurements contain only noise

$$y_i = e_i \tag{2.4b}$$

  implying that the signals θ_i are zero in the noise-only region.

We model the additive noise samples e_i, $i = 1, 2, \ldots, \mathbb{N}_{\text{tot}}$ as zero-mean independent, identically distributed (i.i.d.) Gaussian random variables with known variance σ^2 (which can be easily estimated from the noise-only data). Denote by $\mathcal{N}(y; \mu, \sigma^2)$ the Gaussian probability density function (pdf) of a random variable y with mean μ and variance σ^2. Then, (2.4a) and (2.4b) imply that the conditional distribution of the measurement y_i given θ_i is $p(y_i|\theta_i) = \mathcal{N}(y_i; \theta_i, \sigma^2)$, where $\theta_i = 0$ for $\boldsymbol{s}_i \in \mathcal{R}^{\text{c}}(\boldsymbol{z})$. In the following, we describe a model for the signals θ_i.

C. Defect-Signal (Reflectivity) Model

Assume that the signals θ_i within the defect region [for $\boldsymbol{s}_i \in \mathcal{R}(\boldsymbol{z})$] are i.i.d. Gaussian with unknown mean μ and variance τ^2, which define the vector of unknown *defect-signal distribution parameters*

$$\boldsymbol{w} = [\mu, \tau]^T. \tag{2.5}$$

Therefore, the joint pdf of the defect signals conditional on $\boldsymbol{w}$ and $\boldsymbol{z}$ can be written as

$$p\left(\{\theta_i, \boldsymbol{s}_i \in \mathcal{R}(\boldsymbol{z})\} \,|\boldsymbol{w}, \boldsymbol{z}\right) = \prod_{i, \boldsymbol{s}_i \in \mathcal{R}(\boldsymbol{z})} \mathcal{N}(\theta_i; \mu, \tau^2). \tag{2.6}$$

In the noise-only region (i.e., $\boldsymbol{s}_i \in \mathcal{R}^{\text{c}}(\boldsymbol{z})$), the signals θ_i are zero (see also the previous section).

In the hierarchical modeling context, the elements of $\boldsymbol{w}$ are often referred to as *hyperparameters*. Note that τ is a measure of defect-signal variability: if $\tau = 0$, then all θ_i within the defect region are *equal to* μ.

D. Measurement Model for the Location, Shape, and Defect-Signal Distribution Parameters

Define the vector of all model parameters (see (2.2) and (2.5)), as follows:

$$\boldsymbol{\phi} = [\boldsymbol{z}^T, \boldsymbol{w}^T]^T. \tag{2.7}$$

We now combine the noise and defect-signal models in Sections II-B and II-C and *integrate out* the θ_is. Consequently, conditional on the model parameters $\boldsymbol{\phi}$, the observations y_i collected over the defect region are i.i.d. Gaussian random variables with the following pdf:

$$p(y_i|\boldsymbol{\phi}) = \mathcal{N}(y_i; \mu, \sigma^2 + \tau^2), \qquad \text{for} \quad \boldsymbol{s}_i \in \mathcal{R}(\boldsymbol{z}) \tag{2.8a}$$

whereas the observations collected in the noise-only region are zero-mean i.i.d. Gaussian with pdf:

$$p(y_i|\boldsymbol{\phi}) = \mathcal{N}(y_i; 0, \sigma^2), \qquad \text{for} \quad \boldsymbol{s}_i \in \mathcal{R}^{\text{c}}(\boldsymbol{z}). \tag{2.8b}$$

Since we can *integrate out* the random signals θ_i, $\boldsymbol{s}_i \in \mathcal{R}(\boldsymbol{z})$, we can *decouple* sampling the model parameters $\boldsymbol{\phi}$ from sampling the θ_is, as demonstrated in Sections III-A and III-B.

E. Prior Specifications for the Model Parameters

We assume that the defect location, shape, and signal-distribution parameters are independent *a priori*[2]:

$$\pi_{\boldsymbol{\phi}}(\boldsymbol{\phi}) = \pi_{\boldsymbol{z}}(\boldsymbol{z}) \cdot \pi_{\boldsymbol{w}}(\boldsymbol{w}) \tag{2.9a}$$

where

$$\begin{aligned} \pi_{\boldsymbol{z}}(\boldsymbol{z}) &= \pi_{x_{0,1}}(x_{0,1}) \cdot \pi_{x_{0,2}}(x_{0,2}) \cdot \pi_d(d) \cdot \pi_A(A) \cdot \pi_\varphi(\varphi) \\ \pi_{\boldsymbol{w}}(\boldsymbol{w}) &= \pi_\mu(\mu) \cdot \pi_\tau(\tau). \end{aligned} \tag{2.9b}$$

Let us adopt simple uniform-distribution priors for all the model parameters:

$$\pi_\mu(\mu) = \text{uniform}(0, \mu_{\text{MAX}}) \tag{2.10a}$$
$$\pi_\tau(\tau) = \text{uniform}(0, \tau_{\text{MAX}}) \tag{2.10b}$$
$$\pi_{x_{0,1}}(x_{0,1}) = \text{uniform}(x_{0,1,\text{MIN}}, x_{0,1,\text{MAX}}) \tag{2.10c}$$
$$\pi_{x_{0,2}}(x_{0,2}) = \text{uniform}(x_{0,2,\text{MIN}}, x_{0,2,\text{MAX}}) \tag{2.10d}$$
$$\pi_d(d) = \text{uniform}(d_{\text{MIN}}, d_{\text{MAX}}) \tag{2.10e}$$
$$\pi_A(A) = \text{uniform}(A_{\text{MIN}}, A_{\text{MAX}}) \tag{2.10f}$$
$$\pi_\varphi(\varphi) = \text{uniform}(\varphi_{\text{MIN}}, \varphi_{\text{MAX}}) \tag{2.10g}$$

where $\varphi_{\text{MIN}} \geq -\pi/4$, $\varphi_{\text{MAX}} \leq \pi/4$, $d_{\text{MIN}} > 0$, and $A_{\text{MIN}} > 0$.

III. Bayesian Analysis

The goals of our analysis in this section are to estimate the model parameters $\boldsymbol{\phi}$ and random signals θ_i, $i = 1, 2, \ldots, \mathbb{N}_{\text{tot}}$ describing a single defect region under the measurement model and prior specifications in Section II. The posterior pdf of $\boldsymbol{\phi}$ follows by using (2.8a), (2.8b), and (2.9a):

$$\begin{aligned} p(\boldsymbol{\phi}|\boldsymbol{y}) &\propto \pi_{\boldsymbol{z}}(\boldsymbol{z}) \cdot \pi_{\boldsymbol{w}}(\boldsymbol{w}) \cdot p(\boldsymbol{y}|\boldsymbol{\phi}) \\ &= \pi_{\boldsymbol{z}}(\boldsymbol{z}) \cdot \pi_{\boldsymbol{w}}(\boldsymbol{w}) \cdot \prod_{i, \boldsymbol{s}_i \in \mathcal{R}(\boldsymbol{z})} \mathcal{N}(y_i; \mu, \sigma^2 + \tau^2) \\ &\quad \cdot \prod_{i, \boldsymbol{s}_i \in \mathcal{R}^{\text{c}}(\boldsymbol{z})} \mathcal{N}(y_i; 0, \sigma^2) \\ &\propto \pi_{\boldsymbol{z}}(\boldsymbol{z}) \cdot \pi_{\boldsymbol{w}}(\boldsymbol{w}) \cdot l(\boldsymbol{y}|\boldsymbol{z}, \boldsymbol{w}) \end{aligned} \tag{3.1a}$$

which simply states that the posterior pdf of $\boldsymbol{\phi}$ is proportional to the product of the prior and likelihood of $\boldsymbol{\phi}$. Here, $\boldsymbol{y} = [y_1, y_2, \ldots, y_{\mathbb{N}_{\text{tot}}}]^T$ denotes the vector of all observations,

$$\begin{aligned} &l(\boldsymbol{y}|\boldsymbol{z}, \boldsymbol{w}) \\ &\quad = \prod_{i, \boldsymbol{s}_i \in \mathcal{R}(\boldsymbol{z})} \frac{\mathcal{N}(y_i; \mu, \sigma^2 + \tau^2)}{\mathcal{N}(y_i; 0, \sigma^2)} \\ &\quad = \left(1 + \frac{\tau^2}{\sigma^2}\right)^{-N(\boldsymbol{z})/2} \\ &\qquad \cdot \exp\left\{-\frac{1}{2} \sum_{i, \boldsymbol{s}_i \in \mathcal{R}(\boldsymbol{z})} \left[\frac{(y_i - \mu)^2}{\sigma^2 + \tau^2} - \frac{y_i^2}{\sigma^2}\right]\right\} \end{aligned} \tag{3.1b}$$

[2]Here, $\pi_{\boldsymbol{\phi}}(\boldsymbol{\phi})$ denotes the prior pdf of $\boldsymbol{\phi}$ and analogous notation is used for the prior pdfs of the components of $\boldsymbol{\phi}$.

is the normalized likelihood (i.e., likelihood ratio), and

$$N(\boldsymbol{z}) = \sum_{i,\boldsymbol{s}_i \in \mathcal{R}(\boldsymbol{z})} 1 \tag{3.2}$$

is the number of measurements collected over $\mathcal{R}(\boldsymbol{z})$.

In Sections III-A and III-B (below), we construct methods for drawing samples from the posterior distributions of the model parameters $\boldsymbol{\phi}$ and random signals

$$\boldsymbol{\theta} = [\theta_1, \theta_2, \ldots, \theta_{\mathbb{N}_{\text{tot}}}]^T. \tag{3.3}$$

We utilize these samples to estimate $\boldsymbol{\phi}$ and $\boldsymbol{\theta}$ (Section III-C) and construct credible sets for these parameters.

A. Simulating the Model Parameters $\boldsymbol{\phi}$

We first outline our proposed scheme for simulating from the joint posterior pdf $p(\boldsymbol{\phi}|\boldsymbol{y})$. To draw samples from this distribution, we apply a Gibbs sampler [7]–[9], which utilizes the full conditional posterior pdfs of τ, μ and $\boldsymbol{z}$.

1) Draw $\tau^{(t)}$ from

$$p\left(\tau|\mu^{(t-1)}, \boldsymbol{z}^{(t-1)}, \boldsymbol{y}\right) \tag{3.4a}$$

using *rejection sampling* [7, Ch. 11.1], [10] (as described in Section A of the Appendix), where $\mu^{(t-1)}$ and $\boldsymbol{z}^{(t-1)}$ have been obtained in Steps 2) and 3) of the $(t-1)$th cycle.

2) Draw $\mu^{(t)}$ from

$$p\left(\mu|\tau^{(t)}, \boldsymbol{z}^{(t-1)}, \boldsymbol{y}\right) \tag{3.4b}$$

which is a *truncated Gaussian distribution*, easy to sample from using, e.g., the algorithm in [11] (see also Section B of the Appendix).

3) Draw $\boldsymbol{z}^{(t)}$ from

$$p\left(\boldsymbol{z}|\boldsymbol{w}^{(t)}, \boldsymbol{y}\right) \qquad \text{where} \quad \boldsymbol{w}^{(t)} = \left[\mu^{(t)}, \tau^{(t)}\right]^T \tag{3.4c}$$

using *shrinkage slice sampling* [12] (see Section C of the Appendix).

Cycling through the Steps 1)–3) is performed until the desired number of samples $\boldsymbol{\phi}^{(t)} = [(\boldsymbol{z}^{(t)})^T, (\boldsymbol{w}^{(t)})^T]^T$ is collected [after discarding the samples from the burn-in period (see, e.g., [7]–[9])]. This scheme produces a *Markov chain* $\boldsymbol{\phi}^{(0)}, \boldsymbol{\phi}^{(1)}, \boldsymbol{\phi}^{(2)}, \ldots$ with stationary distribution equal to $p(\boldsymbol{\phi}|\boldsymbol{y})$.

B. Simulating the Random Signals θ_i

To estimate the random signals $\boldsymbol{\theta}$, we utilize *composition sampling* from the posterior pdf $p(\boldsymbol{\theta}|\boldsymbol{y}) = \int p(\boldsymbol{\theta}|\boldsymbol{\phi}, \boldsymbol{y}) p(\boldsymbol{\phi}|\boldsymbol{y}) d\boldsymbol{\phi}$, which can be done as follows (see also [7, steps 1. and 2. on p. 127]):

- draw $\boldsymbol{\phi}^{(t)}$ from $p(\boldsymbol{\phi}|\boldsymbol{y})$, as described in Section III-A;
- draw $\boldsymbol{\theta}^{(t)}$ from $p(\boldsymbol{\theta}|\boldsymbol{\phi}^{(t)}, \boldsymbol{y})$ as follows:
  - for $i \in \mathcal{R}(\boldsymbol{z}^{(t)})$, draw conditionally independent samples $\theta_i^{(t)}$ from

$$p\left(\theta_i^{(t)}|\boldsymbol{\phi}^{(t)}, y_i\right) = \mathcal{N}\left(\theta_i^{(t)}; \frac{\left(\tau^{(t)}\right)^2 y_i + \sigma^2 \mu^{(t)}}{(\tau^{(t)})^2 + \sigma^2}, \left[\frac{1}{(\tau^{(t)})^2} + \frac{1}{\sigma^2}\right]^{-1}\right) \tag{3.5a}$$

  - for $i \in \mathcal{R}^c(\boldsymbol{z}^{(t)})$, set $\theta_i^{(t)} = 0$

yielding $\boldsymbol{\theta}^{(t)} = [\theta_1^{(t)}, \theta_2^{(t)}, \ldots, \theta_{\mathbb{N}_{\text{tot}}}^{(t)}]^T$.

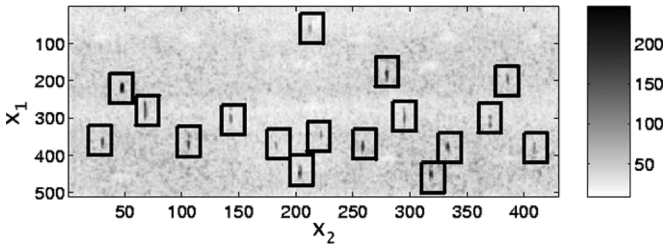

Fig. 1. Ultrasonic C-scan data with 17 defects.

Then, the mean signal $\overline{\theta} = [1/N(\boldsymbol{z})] \cdot \sum_{i,\boldsymbol{s}_i \in \mathcal{R}(\boldsymbol{z})} \theta_i$ within the potential defect region simulated in the tth draw can be estimated as $\overline{\theta}^{(t)} = [1/N(\boldsymbol{z}^{(t)})] \cdot \sum_{i,\boldsymbol{s}_i \in \mathcal{R}(\boldsymbol{z}^{(t)})} \theta_i^{(t)}$.

Note that the proposed MCMC algorithms are *automatic*, i.e., their implementation does not require preliminary runs and additional tuning. This is unlike the Metropolis–Hastings algorithm and algorithms that contain Metropolis steps, which typically require tuning the scales of the proposal distributions [13].

C. Estimating the Model Parameters $\boldsymbol{\phi}$ and Random Signals $\boldsymbol{\theta}$

Once we have collected enough samples, we estimate the posterior means of $\boldsymbol{\phi}$ and $\boldsymbol{\theta}$ simply by averaging the last T draws, as follows:

$$\begin{aligned} \mathrm{E}[\boldsymbol{\phi}|\boldsymbol{y}] &\approx \widehat{\boldsymbol{\phi}} = [\widehat{\boldsymbol{z}}^T, \widehat{\boldsymbol{w}}^T]^T = \frac{1}{T} \sum_{t=t_0+1}^{t_0+T} \boldsymbol{\phi}^{(t)} \\ \mathrm{E}[\boldsymbol{\theta}|\boldsymbol{y}] &\approx \widehat{\boldsymbol{\theta}} = \frac{1}{T} \sum_{t=t_0+1}^{t_0+T} \boldsymbol{\theta}^{(t)} \end{aligned} \tag{3.6}$$

where t_0 defines the burn-in period. Note that $\widehat{\boldsymbol{\phi}}$ and $\widehat{\boldsymbol{\theta}}$ are the (approximate) minimum mean-square error (MMSE) estimates of $\boldsymbol{\phi}$ and $\boldsymbol{\theta}$.

IV. Numerical Examples

We apply the proposed approach to experimental ultrasonic C-scan data from an inspection of a cylindrical Ti 6-4 billet. The sample, developed as a part of the work of the Engine Titanium Consortium, contains 17 #2 flat-bottom holes at $3.2''$ depth. (The flat-bottom holes are machined "defects" whose locations are exactly known.) The ultrasonic data were collected in a single experiment by moving a probe along the axial direction and scanning the billet along the circumferential direction at each axial position. The raw C-scan data with marked true defect regions are shown in Fig. 1. The vertical coordinate is proportional to rotation angle and the horizontal coordinate to axial position.

Before analyzing the data, we divided the C-scan image into three regions of interest, as shown in Fig. 2. In each region, we subtracted row means from the measurements within the same row. We note that the noise level in Region 2 is lower than the corresponding noise levels in Regions 1 and 3. Indeed, the sample estimates of the noise variance σ^2 in Regions 1, 2, and 3 are[3] 11.9^2, 10.3^2, and 12.0^2, respectively. This phenomenon, known as *grain-noise banding* [1], is common in titanium billet inspections; it is a result of the billet manufacturing process. We now analyze each region separately assuming known noise variances σ^2 (set to the above sample estimates). We chose the prior pdfs in (2.10) with $\mu_{\text{MAX}} = \max\{y_1, y_2, \ldots, y_{\mathbb{N}_{\text{tot}}}\}$, $\tau_{\text{MAX}} = 3\sigma$, $d_{\text{MIN}} = 1$, $d_{\text{MAX}} = 10$, $A_{\text{MIN}} = 30$, $A_{\text{MAX}} = 300$, $\varphi_{\text{MIN}} = -\pi/8$,

[3]These sample estimates are computed as follows: $\sigma^2 = (1/\mathbb{N}_{\text{tot}}) \cdot \sum_{i=1}^{\mathbb{N}_{\text{tot}}} y_i^2$. We note that the defects are much smaller in size than the three Regions in Fig. 2; consequently, the defect signals in these regions introduce negligible bias to the estimation of σ^2.

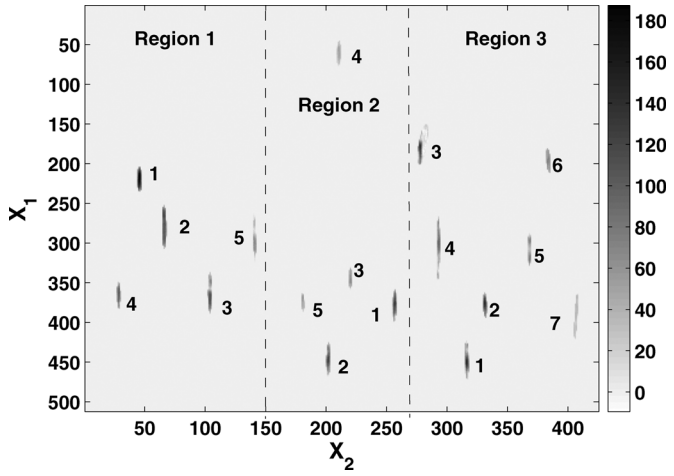

Fig. 2. MMSE estimates $\widehat{\theta}_i$ of the random signals θ_i for the chains having the smallest model-parameter deviances.

$\varphi_{\mathrm{MAX}} = \pi/8$, and selected $x_{0,i,\mathrm{MIN}}$, $x_{0,i,\mathrm{MAX}}$, $i = 1, 2$ to span the region that is being analyzed. The minimum and maximum areas of the defect region (A_{MIN} and A_{MAX}) need to be specified carefully. If we set A_{MAX} to be too large, it may take a long time for our algorithms to converge. If we choose too small A_{MIN}, our chains may converge to some of the grains (in the grain structure of the material), requiring the use of a larger number of chains to ensure that the true defects are not missed.

We now describe our analysis of Region 1, where we ran seven Markov chains. We perform *sequential identification* of potential defects, as described in the following discussion. We first ran 10 000 cycles of the Gibbs sampler described in Section III-A and utilized the last $T = 2000$ samples to estimate the posterior distributions $p(\boldsymbol{\phi}|\boldsymbol{y})$ and $p(\boldsymbol{\theta}|\boldsymbol{y})$; hence, the burn-in period is $t_0 = 8000$ samples. The posterior means $\mathrm{E}[\theta_i|\boldsymbol{y}]$ of the random signals θ_i, which are also the MMSE estimates of θ_i, have been estimated by averaging the T draws (see (3.6)), as follows:

$$\widehat{\theta}_i|_{\text{chain 1}} \approx \frac{1}{T}\sum_{t=t_0+1}^{t_0+T} \theta_i^{(t)}, \qquad i = 1, 2, \ldots, \mathbb{N}_{\mathrm{tot}}. \tag{4.1}$$

Before running the second chain, we *subtracted* the first chain's MMSE estimates $\widehat{\theta}_i|_{\text{chain 1}}$ from the measurements y_i, $i = 1, 2, \ldots, \mathbb{N}_{\mathrm{tot}}$, effectively removing the first potential defect region from the data. We then ran the second Markov chain using the filtered data $y_i|_{\text{chain 2}} = y_i - \widehat{\theta}_i|_{\text{chain 1}}$, computed the MMSE estimates $\widehat{\theta}_i|_{\text{chain 2}}$ of the second potential defect signal (using the second Markov chain), subtracted them out (yielding $y_i|_{\text{chain 3}} = y_i|_{\text{chain 2}} - \widehat{\theta}_i|_{\text{chain 2}}$), and continued this procedure until reaching the desired number of chains. In Fig. 3(a), we show estimated model-parameter deviances (see, e.g., [7, eq. (6.7)])[4]

$$\begin{aligned} d(\boldsymbol{y}, \widehat{\boldsymbol{\phi}}) &= -2\ln p(\boldsymbol{y}|\widehat{\boldsymbol{\phi}}) \\ &= \mathbb{N}_{\mathrm{tot}} \cdot \ln(2\pi\sigma^2) + \sum_{i=1}^{\mathbb{N}_{\mathrm{tot}}} \frac{y_i^2}{\sigma^2} - 2\ln l(\boldsymbol{y}|\widehat{\boldsymbol{z}}, \widehat{\boldsymbol{w}}) \end{aligned} \tag{4.2}$$

for the seven chains in Region 1, where the estimates $\widehat{\boldsymbol{\phi}}$ were computed for each chain using (3.6). The chains have been sorted in the increasing order according to the estimated model-parameter deviances. Note that the true defects have small estimated deviances; hence, we may use these deviances to rank the potential defects according to their severity.

We have applied the proposed sequential scheme to Regions 2 and 3, where we ran seven and ten chains, respectively. The obtained estimated (and sorted) model-parameter deviances for these chains are shown in Fig. 3(b) and (c).

Fig. 2 shows the MMSE estimates of the defect signals for the first five potential defects (chains) from Region 1 (i.e., $\widehat{\theta}_i|_{\text{chain 1}}, \widehat{\theta}_i|_{\text{chain 2}}, \ldots, \widehat{\theta}_i|_{\text{chain 5}}$, see also (4.1)) and first five and seven potential defects from Regions 2 and 3, respectively. The ranks (chain indexes) of the potential defects within each region are also shown in Fig. 2. Remarkably, the locations of these 17 potential defects correspond to the true locations of the flat-bottom holes (i.e., the true defects) in Fig. 1.

Even though the estimated model-parameter deviances in Fig. 3 allow us to assess the severity of potential defect regions, they do not provide sufficient information for deciding between defects and nondefects. To be able to separate defects from nondefects. we need to examine the mean signals and areas of the potential defect regions as well.[5] In Fig. 4, we plot approximate 90% Bayesian confidence regions (credible sets)[6] for the normalized mean signals $\overline{\theta}/\sigma$ and areas A

$$\begin{aligned} &\left([A, \overline{\theta}/\sigma] - [\widehat{A}, \widehat{\overline{\theta}}/\sigma]\right) \\ &\qquad \cdot C^{-1} \cdot \left([A, \overline{\theta}/\sigma]^T - [\widehat{A}, \widehat{\overline{\theta}}/\sigma]^T\right) \le \xi \end{aligned} \tag{4.3}$$

of all 24 potential defects in the three regions.

- $\widehat{A}$ and $\widehat{\overline{\theta}}$ denote the MMSE estimates of A and $\overline{\theta}$ [computed using (3.6)].
- C is the sample covariance matrix of the posterior samples $[A^{(t)}, \overline{\theta}^{(t)}]^T$:

$$\begin{aligned} C = \frac{1}{T} \cdot \sum_{t=t_0+1}^{t_0+T} &\left(\left[A^{(t)}, \frac{\overline{\theta}^{(t)}}{\sigma}\right]^T - \left[\widehat{A}, \frac{\widehat{\overline{\theta}}}{\sigma}\right]^T\right) \\ &\left(\left[A^{(t)}, \frac{\overline{\theta}^{(t)}}{\sigma}\right] - \left[\widehat{A}, \frac{\widehat{\overline{\theta}}}{\sigma}\right]\right). \end{aligned} \tag{4.4}$$

- ξ is a constant chosen (for each chain) so that 90% of the samples $[A^{(t)}, \overline{\theta}^{(t)}]^T$, $t = t_0, \ldots, T$ satisfy (4.3). (A good approximate choice of ξ is $\xi \approx 4$, which is based on the normal-distribution approximation.)

In Fig. 4, we also show that it is possible to separate defects from nondefect using a simple classification boundary $A \cdot (\overline{\theta}/\sigma) - A - 140 = 0$. As the defect-signal strength decreases, the required area (for a real defect) increases; similarly, as the area decreases, the required signal strength increases.

We now present our final example showing the performance of the proposed approach when signal-to-noise ratio is low. Here, we added i.i.d. zero-mean Gaussian noise with variance $\sigma^2 = 250^2$ to the defect signals in Fig. 5(a) (corresponding to one of the flat-bottom holes from the previous examples), yielding the simulated noisy observations in Fig. 5(b). We applied our methods in Sections III-A–III-C to this data set (using (4.1) with $t_0 = 8000$ and $T = 2000$) and obtained the MMSE

[4]See [7, Ch. 6.7], [8, Ch. 6.5.1], and [14] for definitions of deviance-based goodness-of-fit measures and examples of their use.

[5]In NDE applications, estimation of the mean signals and areas of potential defect regions is particularly important for assessing the severity of these regions and their potential to degrade the structural integrity of the test piece.

[6]See e.g., [8, Ch. 2.3.2] for the definition of a credible set. Here, a 90% credible set for $\overline{\theta}/\sigma$ and A is a subset of the space of $\overline{\theta}/\sigma$ and A containing 90% of the probability mass from their posterior pdf.

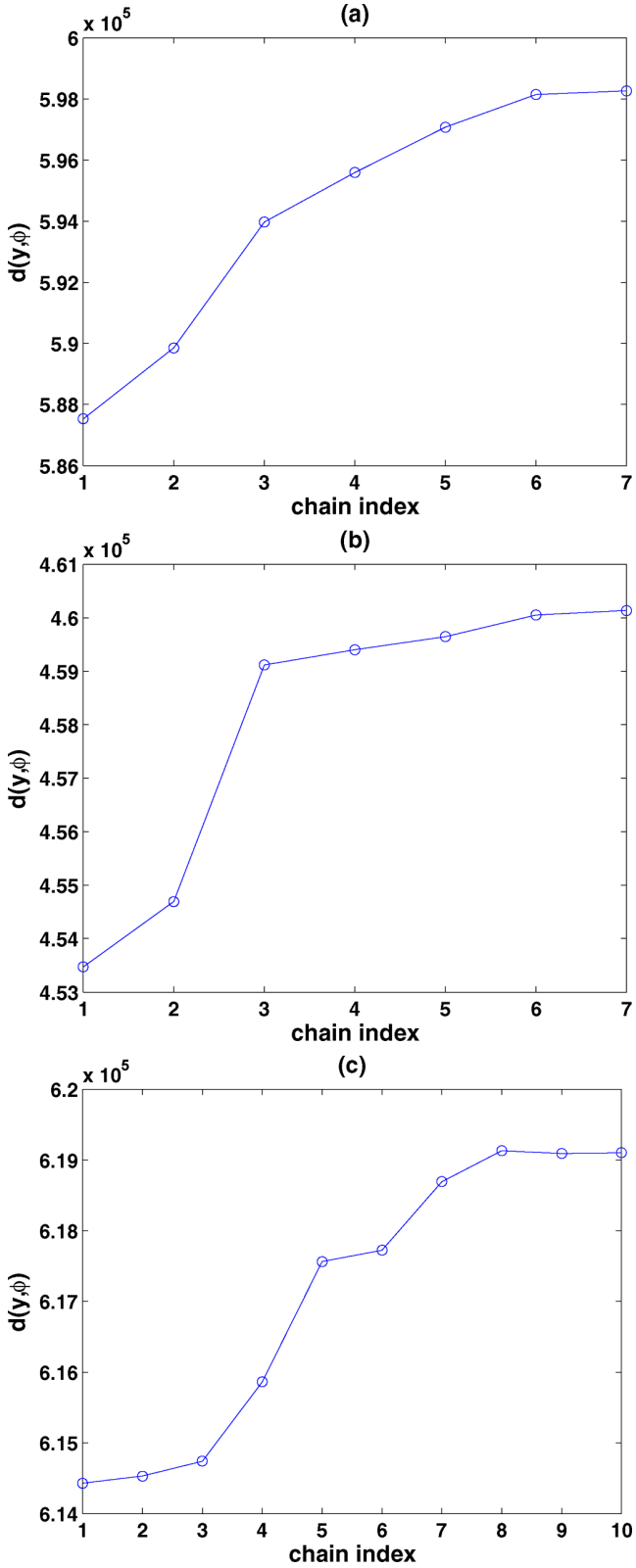

Fig. 3. Estimated model-parameter deviances for the potential defects in Region 1, 2, and 3, respectively. (Color version available online at http://ieeexplore.ieee.org.)

estimates $\widehat{\theta}_i$ shown in Fig. 5(c). The proposed method successfully estimates the defect signal from the noisy measurements.

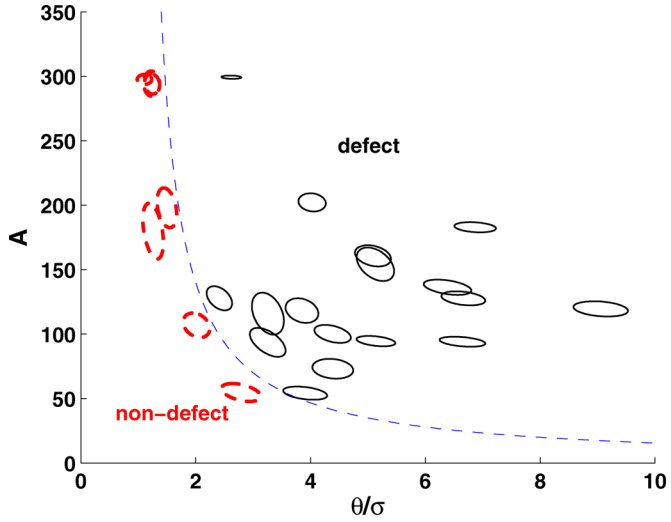

Fig. 4. Approximate 90% credible sets for the normalized mean signals $\overline{\theta}/\sigma$ and areas A of all potential defects in the three regions and a possible classification boundary for separating defects from nondefects. (Color version available online at http://ieeexplore.ieee.org.)

V. Concluding Remarks

We developed a hierarchical Bayesian framework for detecting and estimating NDE defect signals from noisy measurements, derived MCMC methods for estimating the defect signal, location, and shape parameters, and successfully applied them to experimental ultrasonic C-scan data. Our algorithms are automatic and remarkably easy to implement, requiring only the ability to sample from univariate Gaussian, uniform, and exponential distributions.

Further research will include generalizing the proposed approach to correlated signal and noise models.

Appendix A
Implementation of the Gibbs Sampling Steps in Section III-A

A. Step 1) of the Gibbs Sampler: Rejection Sampler

We first derive the full conditional posterior pdf of τ under the measurement model and prior specifications in Sections II-D and II-E. Note that

$$p(\tau|\mu,\boldsymbol{z},\boldsymbol{y}) \propto (\sigma^2+\tau^2)^{-N(\boldsymbol{z})/2} \cdot \exp\left[-\frac{\sum_{i,\boldsymbol{s}_i\in\mathcal{R}(\boldsymbol{z})}(y_i-\mu)^2}{2(\sigma^2+\tau^2)}\right] \cdot i_{(0,\tau_{\mathrm{MAX}})}(\tau) \triangleq q(\tau|\mu,\boldsymbol{z},\boldsymbol{y}) \tag{A.1}$$

where $N(\boldsymbol{z})$ was defined in (3.2) and

$$i_A(x) = \begin{cases} 1, & x \in A \\ 0, & \text{otherwise} \end{cases} \tag{A.2}$$

denotes the indicator function. We utilize *rejection sampling* to simulate τ from $p(\tau|\mu,\boldsymbol{z},\boldsymbol{y})$, as follows:

i) draw τ from $\pi_\tau(\tau) = \text{uniform}(0, \tau_{\mathrm{MAX}})$ (see (2.10b));
ii) draw u from uniform(0, 1);
iii) repeat Steps i) and ii) until

$$u \le \frac{q(\tau|\mu,\boldsymbol{z},\boldsymbol{y})}{\widetilde{m}(\mu,\boldsymbol{z})} \tag{A.3a}$$

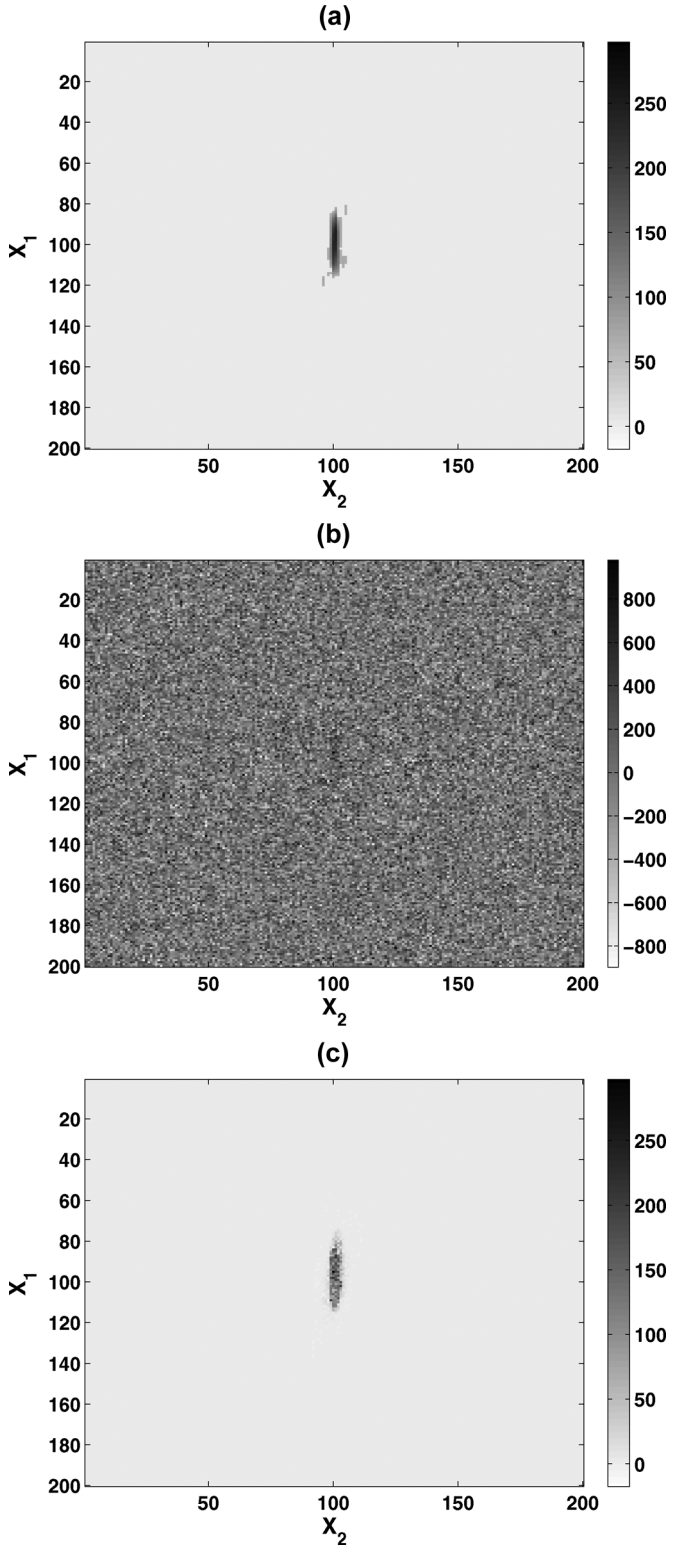

Fig. 5. (a) Signals θ_i, (b) simulated noisy observations y_i, and (c) MMSE estimates $\widehat{\theta}_i$, for $i = 1, 2, \ldots, \mathbb{N}_{\text{tot}}$.

where $\widetilde{m}(\mu, \boldsymbol{z})$ is a bounding constant chosen to guarantee that the right-hand side of the above expression is always between zero and one;

iv) return the τ obtained upon exiting the above loop.

Here, we select

$$\widetilde{m}(\mu, \boldsymbol{z}) = \max_{\tau} q(\tau|\mu, \boldsymbol{z}, \boldsymbol{y}) = q\left(\sqrt{\widehat{\tau}^2(\mu, \boldsymbol{z})}|\mu, \boldsymbol{z}, \boldsymbol{y}\right)$$

where

$$\widehat{\tau}^2(\mu, \boldsymbol{z}) = \min\left\{\max\left[0, \frac{\sum_{i, \boldsymbol{s}_i \in \mathcal{R}(\boldsymbol{z})}^{N(\boldsymbol{z})} (y_i - \mu)^2}{N(\boldsymbol{z})} - \sigma^2\right], \tau_{\text{MAX}}^2\right\}. \tag{A.3b}$$

To draw $\tau^{(t)}$ from the conditional pdf (3.4a), we apply the rejection sampling scheme i)–iv) with μ and $\boldsymbol{z}$ replaced by $\mu^{(t-1)}$ and $\boldsymbol{z}^{(t-1)}$.

B. Step 2) of the Gibbs Sampler

We derive the full conditional posterior pdf of μ under the measurement model and prior specifications in Sections II-D and II-E, as follows:

$$\begin{aligned} p(\mu|\tau, \boldsymbol{z}, \boldsymbol{y}) &\propto \pi_{\mu}(\mu) \cdot \prod_{i, \boldsymbol{s}_i \in \mathcal{R}(\boldsymbol{z})} \mathcal{N}(y_i; \mu, \sigma^2 + \tau^2) \\ &\propto \mathcal{N}\left(\mu; \overline{y}(\boldsymbol{z}), \frac{\sigma^2 + \tau^2}{N(\boldsymbol{z})}\right) \cdot i_{(0, \mu_{\text{MAX}})}(\mu) \end{aligned} \tag{A.4}$$

which is a *truncated Gaussian pdf*. We sample from this pdf using an algorithm similar to that described in [11]. Here, $\overline{y}(\boldsymbol{z}) = [1/N(\boldsymbol{z})] \cdot \sum_{i, \boldsymbol{s}_i \in \mathcal{R}(\boldsymbol{z})} y_i$ is the sample mean of the measurements collected over $\mathcal{R}(\boldsymbol{z})$. To draw $\mu^{(t)}$ from (3.4b), we sample from the truncated Gaussian pdf in (A.4) with τ and $\boldsymbol{z}$ replaced by $\tau^{(t)}$ and $\boldsymbol{z}^{(t-1)}$.

C. Step 3) of the Gibbs Sampler: Shrinkage Slice Sampler

Finally, we discuss sampling from the full conditional posterior pdf of $\boldsymbol{z}$ under the measurement and prior models in Sections II-D and II-E, as follows:

$$p\left(\boldsymbol{z}|\boldsymbol{w}^{(t)}, \boldsymbol{y}\right) \propto \pi_{\boldsymbol{z}}(\boldsymbol{z}) \cdot l\left(\boldsymbol{y}|\boldsymbol{z}, \boldsymbol{w}^{(t)}\right) \tag{A.5}$$

where $l(\boldsymbol{y}|\boldsymbol{z}, \boldsymbol{w})$ was defined in (3.1b). Using the approach in [12], we now construct a *shrinkage slice sampling* algorithm to simulate from the above distribution. We first define the initial (largest) hyperrectangle with limits

$$\begin{aligned} x_{0,1,\text{L}} &= x_{0,1,\text{MIN}}, \quad x_{0,1,\text{U}} = x_{0,1,\text{MAX}} \\ x_{0,2,\text{L}} &= x_{0,2,\text{MIN}}, \quad x_{0,2,\text{U}} = x_{0,2,\text{MAX}} \\ d_{\text{L}} &= d_{\text{MIN}}, \quad d_{\text{U}} = d_{\text{MAX}} \\ A_{\text{L}} &= A_{\text{MIN}}, \quad A_{\text{U}} = A_{\text{MAX}} \\ \varphi_{\text{L}} &= \varphi_{\text{MIN}}, \quad \varphi_{\text{U}} = \varphi_{\text{MAX}} \end{aligned} \tag{A.6}$$

which coincides with the parameter space of $\boldsymbol{\phi}$, see Section II-E. We generate $\boldsymbol{z}^{(t)}$ from (3.4c) as follows:

1) draw an auxiliary random variable $u^{(t)}$ from uniform$(0, l(\boldsymbol{y}|\boldsymbol{z}^{(t-1)}, \boldsymbol{w}^{(t)}))$ pdf;
2) draw $x_{0,1}$ from uniform$(x_{0,1,\text{L}}, x_{0,1,\text{U}})$ pdf, $x_{0,2}$ from uniform$(x_{0,2,\text{L}}, x_{0,2,\text{U}})$, d from uniform$(d_{\text{L}}, d_{\text{U}})$, A from uniform$(A_{\text{L}}, A_{\text{U}})$, and φ from uniform$(\varphi_{\text{L}}, \varphi_{\text{U}})$, yielding $\boldsymbol{z} = [x_{0,1}, x_{0,2}, d, A, \varphi]^T$;
3) check if $\boldsymbol{z}$ is *within the slice*, i.e.,

$$l\left(\boldsymbol{y}|\boldsymbol{z}, \boldsymbol{w}^{(t)}\right) \geq u^{(t)}. \tag{A.7}$$

and if (A.7) holds, return $z^{(t)} = z$ and exit the loop; if (A.7) does not hold, then *shrink the hyperrectangle*, as follows:

- if $x_{0,1} < x_{0,1}^{(t-1)}$, set $x_{0,1,\mathrm{L}} = x_{0,1}$; else if $x_{0,1} > x_{0,1}^{(t-1)}$, set $x_{0,1,\mathrm{U}} = x_{0,1}$;
- if $x_{0,2} < x_{0,2}^{(t-1)}$, set $x_{0,2,\mathrm{L}} = x_{0,2}$; else if $x_{0,2} > x_{0,2}^{(t-1)}$, set $x_{0,2,\mathrm{U}} = x_{0,2}$;
- if $d < d^{(t-1)}$, set $d_{\mathrm{L}} = d$; else if $d > d^{(t-1)}$, set $d_{\mathrm{U}} = d$;
- if $A < A^{(t-1)}$, set $A_{\mathrm{L}} = A$; else if $A > A^{(t-1)}$, set $A_{\mathrm{U}} = A$;
- if $\varphi < \varphi^{(t-1)}$, set $\varphi_{\mathrm{L}} = \varphi$; else if $\varphi > \varphi^{(t-1)}$, set $\varphi_{\mathrm{U}} = \varphi$;
- go back to 2).

Here, the hyperrectangles *shrink toward* $\boldsymbol{\phi}^{(t-1)} = [x_{0,1}^{(t-1)}, x_{0,2}^{(t-1)}, d^{(t-1)}, A^{(t-1)}, \varphi^{(t-1)}]^T$, which is clearly in the slice (see Step 1)).

Since the evaluation of $l(\boldsymbol{y}|\boldsymbol{z}, \boldsymbol{w})$ may cause a floating-point underflow, it is often safer to compute $\ln l(\boldsymbol{y}|\boldsymbol{z}, \boldsymbol{w})$ and modify the above algorithm accordingly (see [12, Sec. 4]).

ACKNOWLEDGMENT

The authors would like to thank the anonymous reviewers and to Prof. R. B. Thompson from CNDE, Iowa State University, for their insightful comments and for bringing [1] and [6] to our attention.

REFERENCES

[1] P. J. Howard, D. C. Copley, and R. S. Gilmore, "The application of a dynamic threshold to C-scan images with variable noise," in *Rev. Progress Quantitative Nondestructive Evaluation*, D. O. Thompson and D. E. Chimenti, Eds. Melville, NY: Amer. Inst. Phys., 1998, vol. 17, pp. 2013–2019.

[2] A. Tsai, A. Yezzi, Jr., and A. S. Willsky, "Curve evolution implementation of the Mumford–Shah functional for image segmentation, denoising, interpolation, and magnification," *IEEE Trans. Image Process.*, vol. 10, pp. 1169–1186, Aug. 2001.

[3] D. L. Pham, C. Y. Xu, and J. L. Prince, "Current methods in medical image segmentation," *Annu. Rev. Biomed. Eng.*, vol. 2, pp. 315–337, 2000.

[4] W. E. Polakowski *et al.*, "Computer-aided breast cancer detection and diagnosis of masses using difference of Gaussians and derivative-based feature saliency," *IEEE Trans. Med. Imag.*, vol. 16, pp. 811–819, Sep. 1997.

[5] A. Dogandžić and B. Zhang, "Bayesian defect signal analysis," in *Rev. Progress Quantitative Nondestructive Evaluation*. Melville, NY: Amer. Inst. Phys., 2006, vol. 25, pp. 617–624.

[6] Aerospace Industries Association Rotor Integrity Sub-Committee, "The development of anomaly distributions for aircraft engine titanium disk alloys," in *Proc. 38th AIAA/ASME/ASCE/AHS/ASC Structures, Structural Dynamics, Materials Conf.*, Kissimmee, FL, Apr. 1997, pp. 2543–2553 [Online]. Available: http://www.darwin.swri.org/html_files/pdf_docs/pubs/aia1997.pdf

[7] A. Gelman, J. B. Carlin, H. S. Stern, and D. B. Rubin, *Bayesian Data Analysis*, 2nd ed. New York: Chapman & Hall, 2004.

[8] B. P. Carlin and T. A. Louis, *Bayes and Empirical Bayes Methods for Data Analysis*, 2nd ed. New York: Chapman & Hall, 2000.

[9] C. P. Robert and G. Casella, *Monte Carlo Statistical Methods*, 2nd ed. New York: Springer-Verlag, 2004.

[10] J. von Neumann, "Various techniques used in connection with random digits," in *John von Neumann, Collected Works*. New York: Pergamon, 1961, vol. V, pp. 768–770.

[11] J. Geweke, "Efficient simulation from the multivariate normal and student-t distributions subject to linear constraints," in *Computing Science Statistics: Proc. 23rd Symp. Interface*, Seattle, WA, Apr. 1991, pp. 571–578.

[12] R. M. Neal, "Slice sampling," *Ann. Statist.*, vol. 31, pp. 705–741, Jun. 2003.

[13] C. Andrieu, A. Doucet, and C. P. Robert, "Computational advances for and from Bayesian analysis," *Stat. Sci.*, vol. 19, no. 1, pp. 118–127, Feb. 2004.

[14] D. J. Spiegelhalter, N. G. Best, B. R. Carlin, and A. van der Linde, "Bayesian measures of model complexity and fit," *J. R. Stat. Soc.*, ser. B, vol. 64, pp. 583–639, 2002.

Attenuation Estimation From Correlated Sequences

Tarek Medkour and Andrew T. Walden

***Abstract*—We calculate the frequency-dependent variance of the log spectral ratio for correlated time series. This is used to produce a weighted least-squares approach to attenuation estimation, with weights calculated from estimated coherence. Applications to synthetic and real data illustrate that, for correlated series, the method improves significantly on traditional unweighted least-squares attenuation estimates.**

***Index Terms*—Attenuation, coherence, correlation, spectral ratios.**

I. INTRODUCTION

Attenuation can be estimated from the change in frequency content observed between two sequences separated by two-way travel time ΔT (e.g., [14] and [16]).

Given power spectra $S_{11}(f)$ and $S_{22}(f)$ corresponding to the sequences $\{X_{1,t}\}$ and $\{X_{2,t}\}$, we define the attenuation parameters through the spectral ratio as follows, $S_{22}(f)/S_{11}(f) = c_0 \cdot \exp[-2\,\Delta T\,\alpha(f)]$, where $\alpha(f)$ is the attenuation coefficient and c_0 is a constant. The acoustic attenuation coefficient of soft biological tissue has been observed to have a linear-with-frequency characteristic [7]. Likewise a linear form has also been justified in seismology [4], [17], and the ubiquitous linear assumption for attenuation is made in this correspondence. Let $\alpha(f) = \mu f$ say, where μ is a constant, so that

$$\log\left[\frac{S_{22}(f)}{S_{11}(f)}\right] = c - 2\,\Delta T\,\mu f \tag{1}$$

where $c = \log c_0$ and the coefficient μ is called the logarithmic decrement and is measured in nepers (better known as the natural log of a voltage ratio). Since $\alpha(f) = \mu f$, by slight abuse of notation (we are using time not distance) $\alpha(f)$ has units of nepers/wavelength. In terms of the oft-used quality factor $Q(f)$, (1) can be written

$$\log\left[\frac{S_{22}(f)}{S_{11}(f)}\right] = c - \frac{2\pi\Delta T\, f}{Q} \tag{2}$$

so that $\mu = \pi/Q$ and $\alpha(f) = \mu f = \pi f/Q$. Since one neper is equivalent to $20\log_{10} e$ dB ≈ 8.686 dB, it is apparent that $\alpha(f) \approx (27.3/Q)f$ dB/wavelength.

While in attenuation studies via spectral ratios, it is invariably assumed that the sequences involved are independent, [3], [8], here we will consider estimation of the quality factor, Q, when the sequences are correlated.

When the log spectral ratio in (2) is estimated via multitapering, it is seen in Section II that at any frequency, this ratio can be viewed as a log variance ratio in complex Gaussian random variables. This is explored in Section III where the distribution of the estimated log spectral ratio (standardized by the true ratio) is developed, and, most important, its cumulant generating function, and hence variance, are derived. This frequency-dependent variance is a decreasing function of the ordinary coherence—which reflects sequence correlation—between the two sequences. Section IV sets up the regression model through which

Manuscript received October 3, 2005; revised April 4, 2006. The associate editor coordinating the review of this manuscript and approving it for publication was Dr. A. Rahim Leyman. T. Medkour thanks the government of the People's Democratic Republic of Algeria for financial support.

The authors are with the Department of Mathematics, Imperial College London, London SW7 2BZ, U.K. (e-mail: tarek.medkour@imperial.ac.uk and a.walden@imperial.ac.uk).

Digital Object Identifier 10.1109/TSP.2006.885682